ADVANCED MATERIALS

www.advmat.de

Homojunction of Oxygen and Titanium Vacancies and its Interfacial n–p Effect

Si-Ming Wu, Xiao-Long Liu, Xi-Liang Lian, Ge Tian, Christoph Janiak, Yue-Xing Zhang, Yi Lu, Hao-Zheng Yu, Jie Hu, Hao Wei, Heng Zhao, Gang-Gang Chang, Gustaaf Van Tendeloo, Li-Ying Wang, Xiao-Yu Yang, and Bao-Lian Su*

The homojunction of oxygen/metal vacancies and its interfacial n–p effect on the physiochemical properties are rarely reported. Interfacial n–p homojunctions of TiO_2 are fabricated by directly decorating interfacial p-type titanium-defected TiO_2 around n-type oxygen-defected TiO_2 nanocrystals in amorphous–anatase homogeneous nanostructures. Experimental measurements and theoretical calculations on the cell lattice parameters show that the homojunction of oxygen and titanium vacancies changes the charge density of TiO_2; a strong EPR signal caused by oxygen vacancies and an unreported strong titanium vacancies signal of 2D ^{1}H TQ-SQ MAS NMR are present. Amorphous–anatase TiO_2 shows significant performance regarding the photogeneration current, photocatalysis, and energy storage, owing to interfacial n-type to p-type conductivity with high charge mobility and less structural confinement of amorphous clusters. A new "homojunction of oxygen and titanium vacancies" concept, characteristics, and mechanism are proposed at an atomic-/nanoscale to clarify the generation of oxygen vacancies and titanium vacancies as well as the interface electron transfer.

Titanium dioxide, TiO_2, as one of the most attractive semiconductors for photocatalysis, energy storage, and solar fuel technologies,[1–5] is a nonstoichiometric compound and generally known to be an oxygen-deficient compound, TiO_{2-x}, whose n-type semiconducting properties are associated with oxygen vacancies (O-vacancies) and titanium interstitials.[6,7] Defects of TiO_2 also include titanium vacancies (Ti-vacancies) that form acceptor type centers responsible for p-type properties.[8,9] The n–p junction is considered as a very promising structure to promote charge separation and thus improve the photo/electro performance of semiconductors.[10] The homojunction of oxygen and titanium vacancies might therefore provide TiO_2 with unidirectional conductivity from n-type to p-type, which can enhance the electron conductivity and charge transport properties of TiO_2. From a stoichiometric point of view and from the macroscopic properties, however, a p-type Ti-vacancies in an n-type TiO_2 semiconductor is theoretically and technologically irrational; the homojunction of O-vacancies and Ti-vacancies therefore seems impossible in normal n-type TiO_2 without a foreign phase. Calcination is the most common approach for engineering TiO_2 defects, O-vacancies as well as Ti-vacancies.[11,12] The only difference is that O-vacancies are caused by an oxygen escape and Ti-vacancies are obtained from an oxygen-rich (O-rich) environment. Therefore, a homojunction of O-vacancies and Ti-vacancies is theoretically

S.-M. Wu, X.-L. Lian, Dr. G. Tian, Y. Lu, H.-Z. Yu, J. Hu, H. Wei, H. Zhao, Dr. G.-G. Chang, Prof. X.-Y. Yang, Prof. B.-L. Su
State Key Laboratory of Advanced Technology for Materials Synthesis and Processing
Wuhan University of Technology
122, Luoshi Road, Wuhan 430070, China
E-mail: xyyang@seas.harvard.edu, xyyang@whut.edu.cn

Prof. X.-L. Liu, Prof. L.-Y. Wang
State Key Laboratory of Magnetic Resonance and Atomic and Molecular Physics
Wuhan Institute of Physics and Mathematics
The Chinese Academy of Sciences
Wuhan 430071, China

Prof. C. Janiak
Institut für Anorganische Chemie und Strukturchemie
Heinrich-Heine-Universität Düsseldorf
40204 Düsseldorf, Germany

Prof. Y.-X. Zhang
Hubei Collaborative Innovation Center for Advanced Organic Chemical Materials
Ministry of Education Key Laboratory for the Synthesis and Application of Organic Functional Molecules
College of Chemistry and Chemical Engineering
Hubei University
Wuhan 430062, China

Prof. G. Van Tendeloo
EMAT (Electron Microscopy for Materials Science)
University of Antwerp
Groenenborgerlaan 171, B-2020 Antwerpen, Belgium

Dr. X.-Y. Yang
School of Engineering and Applied Sciences
Harvard University
Cambridge, MA 02138, USA

Prof. B.-L. Su
Laboratory of Inorganic Materials Chemistry (CMI)
University of Namur
61, rue de Bruxelles, B-5000 Namur, Belgium

DOI: 10.1002/adma.201802173

possible in a single crystal, because the escaping/migrating oxygen from O-vacancies can be used to form an O-rich interface for producing Ti-vacancies. The homojunction of O-vacancies and Ti-vacancies by calcination can not only develop a low-cost approach to practical applications but also shed new light on the fundamental aspects of the semiconductor nature. A very careful control of the calcination temperature has been widely used to synthesize high-performance TiO_2.[13–16] However, there are very limited studies on the nature of TiO_2, directly caused by calcination. It has to be pointed out that this theoretical homojunction of O-vacancies and Ti-vacancies is very difficult to be detected by a single characterization, because of the simultaneous observation of atomic-/nanoscaled Ti-vacancy defects in the macroscaled O-vacancy phases, especially in a full-crystalline phase junction[17] or facet junction.[18]

In order to better understand the role of native defects and the unique phenomena of a homojunction of O-vacancies and Ti-vacancies, amorphous–anatase homojunctions are mostly preferred, because a relatively small amount of Ti-vacancies might form in the interfacial O-rich environment caused by the lattice/surface oxygen escape/migration during grain-boundary migration from the anatase to the amorphous phase.[19,20] Moreover, amorphous TiO_2 nanoclusters as homojunction-phase on bulky crystals can act as hole-trapping sites in photocatalysis[21–23] and delamination resistant in lithium/sodium storage for performances enhancement.[12] There are also many successful amorphous nanocluster interfacial bonding nanostructures having advantageous features such as amorphous interfacial stability,[24] quantized electrical transport,[25] and rich edge-atoms of amorphous–crystalline phase.[26,27] It is scientifically interesting to fabricate amorphous nanoclusters as interfacial bonding of TiO_2 nanocrystals; they can form a model of the homojunction of O-vacancies and Ti-vacancies in pure TiO_2, functioning without incorporating foreign phases and/or ions into the TiO_2 lattice.

Multiple techniques have been applied for the detection of O-vacancies and Ti-vacancies such as high resolution transmission electron microscopy (HRTEM), electron paramagnetic resonance (EPR), X-ray photoelectron spectroscopy (XPS) or the macroscopic property of p-type semiconductors such as Mott–Schottky measurement. However, the interfacial Ti-vacancy state in the n-type TiO_2 semiconductor is quite difficult to be directly characterized because of the low amount, the weak signal and the indefinite structure. Titanol (Ti—OH) sites often occur on the surface and interface of TiO_2 and are therefore chosen to be probe species to detect the very low amounts of Ti-vacancies by 2D ^{1}H TQ-SQ magic-angle spinning (MAS) NMR. The latter is a powerful tool to probe homonuclear proton–proton spatial proximities and allows to observe the resonances with very close or even identical isotropic chemical shifts.[28,29] Microporous TiO_2 beans as starting materials have been synthesized by an ultrafast (about 30 s) and templating-free approach, which results in completely amorphous structures and absence of organic templates. A homojunction of O-vacancies and Ti-vacancies can be prepared by careful control of the calcination. Thermogravimetric analysis-differential thermal analysis (Figure S1, Supporting Information) indicates a phase transformation when heating around 250–300 °C; because the free energy of the transformation from amorphous

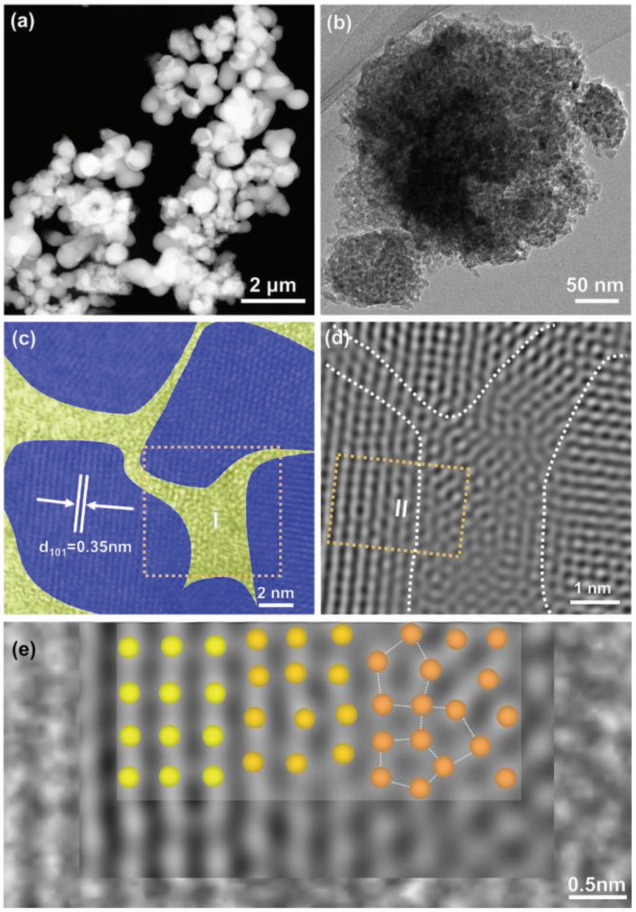

Figure 1. a) STEM image of TiO_2-350. b,c) TEM image (b) and HRTEM image (c) of TiO_2-350. d) Inverse FFT of region I in (c) showing crystal fusion domains of TiO_2. e) Original TEM image and inverse FFT of region II, and the corresponding atomic models of highly crystalline phase (ordered lattice, light yellow, left), nanofusion phase (dark yellow, middle), and semicrystalline/amorphous phase (disordered defect, brown, right).

to anatase TiO_2 is negative above 400 °C, and the transformation from amorphous to anatase TiO_2 is irreversible.[30,31] 350 °C is chosen to obtain a metastable anatase phase in an amorphous–anatase composite. With increasing heating temperature, for comparison, TiO_2-450, TiO_2-550, TiO_2-650, TiO_2-750, and TiO_2-850 have been obtained. The surface morphology of the beads shows notable changes from smooth to aggregation (Figure S2, Supporting Information), and the nanoparticles form beans with a size of 500 nm and step-growth in size and crystallinity (**Figure 1**a; Figures S2–S4, Supporting Information), as well as phase transformation[30] (Figure S5, Supporting Information). The pore sizes increase and the Brunauer–Emmett–Teller (BET) surface areas and pore volumes decrease (Figure S6, Table S1, Supporting Information).

The beads of TiO_2-350 shown in Figure 1a have a uniform diameter of about 500–600 nm and consist of uniform nanoparticles with a diameter of about 15 nm (Figure 1b). The HRTEM image (Figure 1c; Figure S7a,b, Supporting Information) shows that the lattice fringes of 0.35 nm of TiO_2-350 agree with the anatase titania (101) interplanar spacing. The nanocrystals with a size of around 8–10 nm (Figure 1c, blue areas) are bonded

together by an interconnecting amorphous/semicrystalline interface of around 1–4 nm (Figure 1c, yellow areas). The amorphous/semicrystalline/highly crystalline phase can be very well visualized from the HRTEM image and the inverse fast Fourier transformation (FFT) in Figure 1d,e and Figure S7c–e (Supporting Information). The ordered lattice fringes at the left, the lattice distortions at the middle, and the disordered amorphous phase at right are clearly discerned. This highly crystalline/semicrystalline/amorphous phase is coherent at the atomic scale, and defect generation mainly occurs at the interface region. The thickness of the nanointerface is around 2–4 nm, which allows the ballistic transport of quantized electrical conductance.[24] The crystalline and amorphous homogeneous nanostructures intersect at atom level as a larger fusion particle, creating what Chaos Theory describes as the fabric of the network of brains,[32,33] which means that these nanostructures of so-called chaos materials are the minimum cross section for electron transport and minimum interface-losing of energy.

To obtain information about the oxygen vacancies, EPR spectra are recorded (**Figure 2**). For TiO_2-350, the sharp peak with the corresponding $g_{yy} = 2.001$ is assigned to oxygen vacancies[34] and the highest intensity means that TiO_2-350 has the highest level of oxygen vacancies of all the samples treated at different temperatures. The EPR signals at $g_{zz} = 2.020$ and $g_{xx} = 1.98$ can be attributed to O_2^- and Ti^{3+}.[35] Moreover, the positive slope of the linear part of the Mott–Schottky plots (Figure S8, Supporting Information) confirms the n-type conductivity of TiO_2-350. Notably, there is little difference between

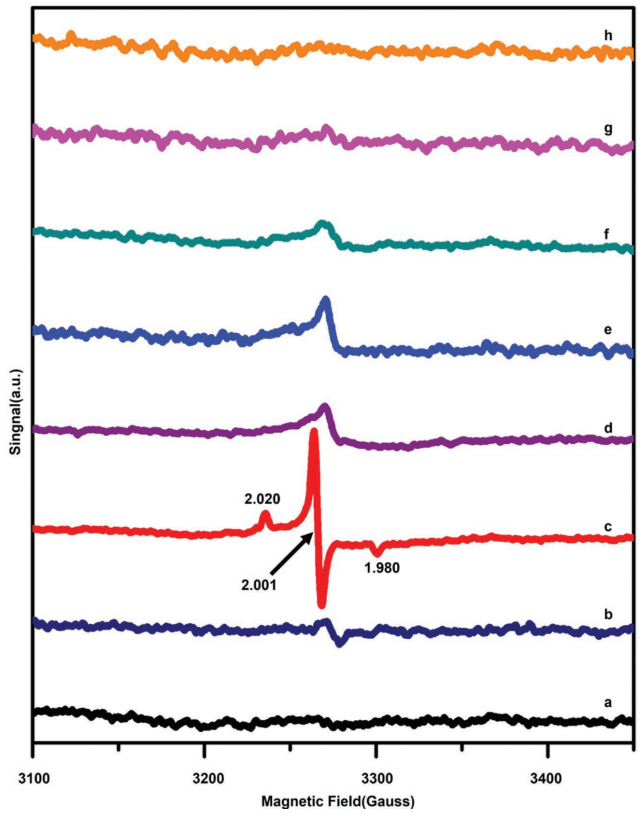

Figure 2. EPR spectra of: a) TiO_2-A, b) TiO_2-250, c) TiO_2-350, d) TiO_2-450, e) TiO_2-550, f) TiO_2-650, g) TiO_2-750, and h) TiO_2-850.

TiO_2-350 and TiO_2-550 as to microscopic morphology, bead size, crystal phase, or mesoporous structure. The only change is that TiO_2-350 has an elaborated structure interface between the amorphous and the anatase phase (Figure 1c). In contrast, for TiO_2-550 there are few interface areas because of almost no or very small amorphous clusters (Figure S3d, Supporting Information). Therefore, most of the oxygen vacancies should be present at the interface between the amorphous clusters and the anatase nanocrystals.

The interfacial Ti-vacancies state we expect is quite difficult to directly characterize because of the low amount, the weak EPR signal, and indefinite structure. Basically, the −OH sites in oxides can be categorized into three distinctively different species: I) occurring at the surface, II) broken M−O−M bonds, and III) metal vacancies. Titanol (Ti−OH) sites can therefore act as probe species to detect the Ti-vacancies by NMR, which are shown in **Figure 3**A: I) surface Ti-OH; II) Ti−OH from broken Ti−O−Ti bonds in the bulk; III) Ti−OH nests from the Ti-vacancies. Ti-OH groups in Ti-OH nests would be stabilized by hydrogen bonds and the formation of Ti−OH nests can effectively stabilize the clusters with negative oxygen.

To determine the defects in TiO_2, we performed highly sophisticated pulse techniques such as 2D ^{1}H TQ-SQ MAS NMR methods, which are not affected by the water signal. The hydrogen bond network can exert a large influence on the FT-IR and ^{1}H NMR chemical shift of Ti-OH (Figures S9, S10, Supporting Information) and gives rise to a low-field shift of the resonance lines.[36] Note that a cluster of three protons is mandatory for the occurrence of a TQ coherence. Pairs of off-diagonal peaks at (δa, δa + δb + δc), (δb, δa + δb + δc), and (δc, δa + δb + δc) correspond to correlations between three protons with different chemical shifts. The signal of Ti−OH groups from broken Ti−O−Ti bonds in the bulk phase appears in the range from 6.5 to 8.9 ppm in Figure 3, and the range from 1.2 to 3.5 ppm is assigned to the location of Ti−OH groups at the surface.

The signal at (7.10, 7.10 + 7.10 + 1.84) in Figure 3B-a demonstrates that in TiO_2-A there are Ti-OH species near the solid surface with $\delta_H = 1.84$ ppm, and Ti−OH species from broken Ti−O−Ti bonds with $\delta_H = 7.10$ ppm which were forming hydrogen bonds. At 250 °C, the signal at (6.00, 6.00 + 6.00 + 6.00) (Figure 3B-b) shows that Ti-vacancies start to form, and Ti−OH species from broken Ti−O−Ti bonds and surface Ti−OH groups are in the phases. When the heating temperature reaches 350 °C, Ti−OH nests are kept and almost no other Ti−OH species are present in the bulk (Figure 3B-c). Further increasing the temperature only causes the loss of Ti−OH nests, and only Ti−OH species from broken Ti−O−Ti bonds and surface Ti−OH species can be observed (see detailed description of ^{1}H TQ-SQ MAS NMR in Supporting Information).

For a better understanding of the nature of the homojunction of Ti-vacancies and O-vacancies, the experimental data and theoretical computations (XPS, transient photocurrent responses and density functional theory) have been further used to study the role of the amorphous interface.

The Ti 2p and O1s core-level XPS spectra (Figure S11a,b, Supporting Information) show obvious Ti^{3+} (457.5 eV in Ti 2p XPS)[12,37,38] and O^- species (around 531.2 eV O1s XPS)[39,40] as shoulder peaks. An interesting difference of TiO_2-350, TiO_2-550,

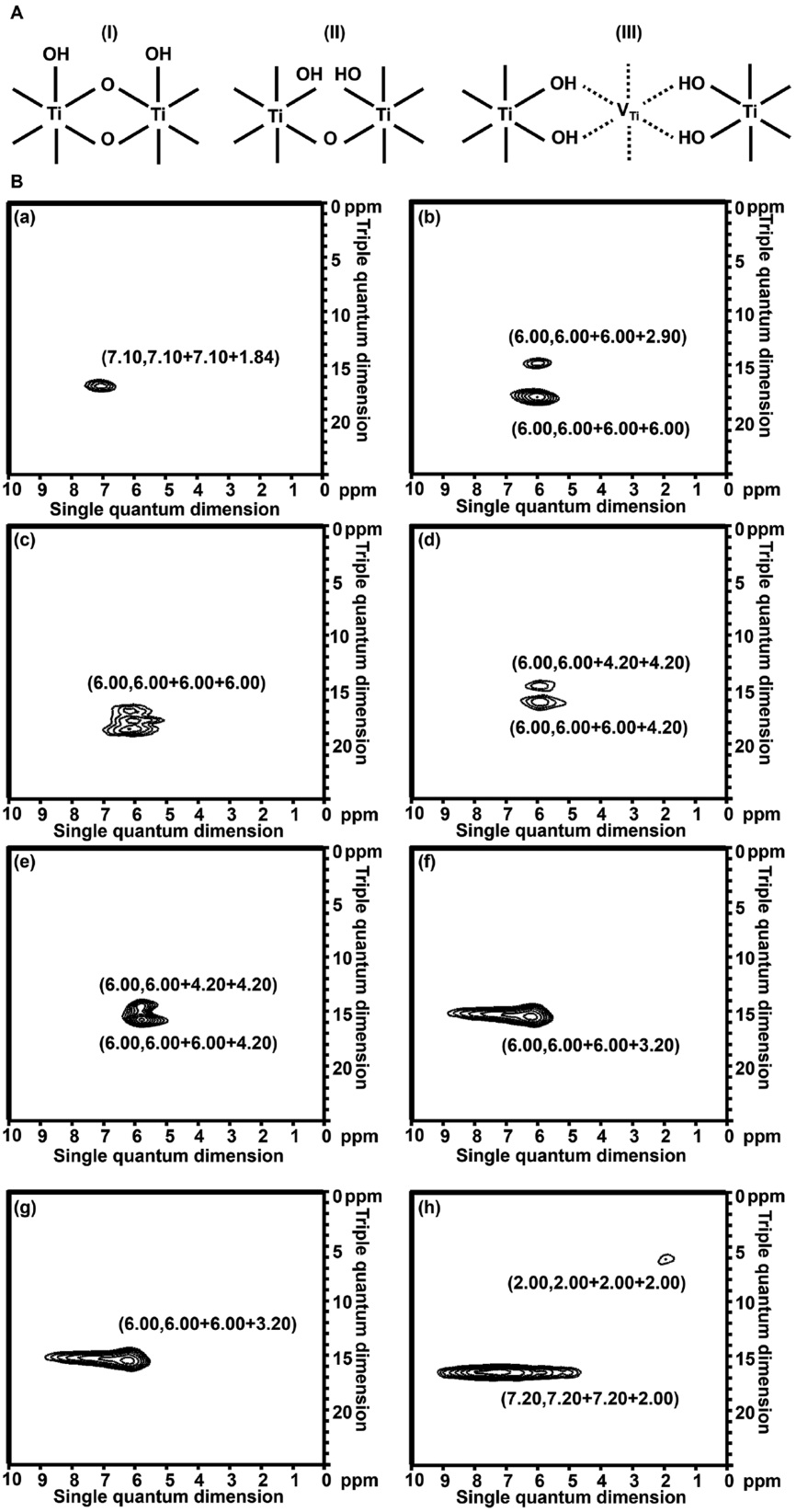

Figure 3. A) Proposed OH species in TiO_2. I refers to surface Ti—OH species; II refers to Ti—OH species from broken Ti—O—Ti bonds; III refers to Ti-OH nests from Ti vacancies. B) ^{1}H TQ-SQ MAS NMR spectra of: a) TiO_2-A, b) TiO_2-250, c) TiO_2-350, d) TiO_2-450, e) TiO_2-550, f) TiO_2-650, g) TiO_2-750, and h) TiO_2-850.

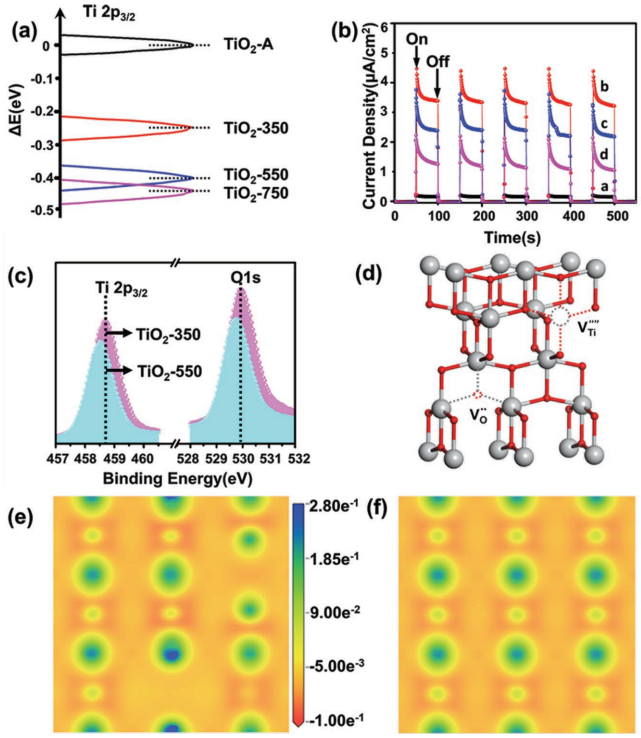

Figure 4. a) Ti $2p_{3/2}$ chemical shift among TiO_2-A, TiO_2-350, TiO_2-550, and TiO_2-750. b) Transient photocurrent responses of: (a) TiO_2-A, (b) TiO_2-350, (c) TiO_2-550, and (d) TiO_2-750 vs SCE under UV–vis light irradiation. c) Ti $2p_{3/2}$ and O 1s XPS spectra of TiO_2-350 and TiO_2-550. d) Simulated geometric structures of TiO_2 with junction of O-vacancies and Ti-vacancies. e,f) Charge density difference of TiO_2 with junction of O-vacancies and Ti-vacancies (e) and normal TiO_2 (f).

and TiO_2-750 is provided by the Ti 2p chemical shift (**Figure 4**a) of 0.3, 0.4, and 0.5 eV, respectively, compared to that of TiO_2-A, which describes the change of the chemical environments and phase varieties.[41,42] The binding energy of Ti $2p_{3/2}$ of TiO_2-350 is between the amorphous phase (TiO_2-A) and anatase phase (TiO_2-550), directly due to its coherent amorphous–anatase homostructure at an atomic level. This is in very good agreement with the results of the phase ratio calculated by XRD data (Figure S12, Supporting Information), TEM data, and the similar O1s chemical shift (Figure S11c,d, Supporting Information).

It is also apparent that the current density of TiO_2-350 is 3.5 μA cm^{-2}, which is 1.4-fold of TiO_2-550 (n-type anatase phase), 2.7-fold of TiO_2-750 (n-type anatase-rutile phase-junction), and 16-fold of TiO_2-A (amorphous phase) (Figure 4b). For n-type TiO_2, the photocurrent intensity mainly depends on the amount of O vacancies. Notably, the molar ratio of Ti/O (0.53 ± 0.02 of TiO_2-350) is essentially equal to that of TiO_2-550 (Ti/O = 0.54 ± 0.02) (Figure S13, Supporting Information), meaning that the amount of lattice oxygens in TiO_2-350 is near that of TiO_2-550. This is due to the fact that the presence of Ti-vacancies in TiO_2-350 would balance the O-vacancies. We further calculated the charge density of the junction mode of O-vacancies and Ti-vacancies (Figure 4e). The neighboring O and Ti atoms of O-vacancy get more electrons, while less electrons are shown in the neighboring atoms of Ti-vacancy, in comparison with those on the normal sites (Figure 4f). Ti-vacancies are an acceptor type intrinsic defect, so the presence of interfacial Ti-vacancies may lead to a fast electronic transmission from interface n to interface p. Such a unique n–p electronic transmission is mostly preferred for the mobility of electronic charge carriers in application of photocatalysis and storage of lithium/sodium cations. Apart from the amorphous/anatase TiO_2-350 with a phase ratio of around 0.24 (Figure S12, Supporting Information) we have also tested photoactivity (Figure S14, Supporting Information) and photocatalytic activity in liquid/gas degradation and storages of lithium/sodium ions and compared to TiO_2 constructed by amorphous nanoparticles (TiO_2-A), n-type anatase TiO_2 (TiO_2-550), rutile/anatase TiO_2 (phase ratio around 0.25, TiO_2-750), mixed amorphous-crystalline TiO_2 (mixed TiO_2), and other commercial TiO_2 nanomaterials (nano-TiO_2 and TiO_2 nanotube) (Figure S15, Supporting Information). Obviously, TiO_2-350 is significantly more active than TiO_2-A, TiO_2-550, TiO_2-750, mixed TiO_2, and other commercial TiO_2 nanomaterials (up to 3-fold the photocatalytic activity and 3.5-fold the Na^+ capacity in comparison with n-type TiO_2), for example, 2-fold, 1.4-fold, 1.6-fold, and 1.9-fold of TiO_2-550 in MB/acetone degradation, and Li^+/Na^+ capacity. Further investigation of the photocatalytic stability of TiO_2-350 shows around 93% of photocatalytic activity is retained after five cycles of photocatalysis (Figure S15d, Supporting Information), and the strong signal of the O-vacancies from EPR and the Ti-vacancies from 2D ^{1}H TQ-SQ MAS NMR can be clearly observated (Figure S15e,f, Supporting Information), suggesting the high stability of the homojuction of O-vacancies and Ti-vacancies.

The proposed formation mechanism and photo/electro performance mechanism of TiO_2-350 are shown in **Figure 5**. The amorphous nanoparticles allow a controlled nanofusion and nanocrystal growth, and the microporous structure offers defined grain-boundaries, high porosity, and growth space, which could prevent nanocrystals from overgrowth and/or overfusion at certain calcination temperatures. Firstly, the nanoparticles aggregate, micropores disappear, nanoclusters appear and grow, and nanofusion domains form during the early stage of calcination at 350 °C (from Figure 5A-a to b, middle). Meanwhile, the O atoms often trend to escape/migrate from the lattice when crystalline anatase form, resulting in n-type TiO_2. The rearrangement of Ti and O atoms starts, the lattice phase forms, the migrating O species (possible including surface oxygen, interstitial oxygen, and/or lattice oxygen) escape/migrate to form O-vacancies and the Ti species near O-vacancies would be Ti^{3+} to balance the loss of O atoms. The formation of oxygen vacancies in TiO_2 could be related to the reduced energy required for the escape and/or migration of the O species from the lattice due to the atomic/nanoscaled thermodynamic effect.[43] Using the Kröger–Vink notation,[44] the formation of oxygen vacancies can be expressed as

$$O_O \rightarrow V_O^{\bullet\bullet} + 2e' + O_M^x \quad (1)$$

$$O_O \rightarrow V_O^{\bullet\bullet} + 2e' + \frac{1}{2}O_2 \quad (2)$$

where O_O represents lattice oxygen, $V_O^{\bullet\bullet}$ represents oxygen vacancy, e′ represents electron charge, and O_M^x represents migrating oxygen of a dynamic state/balance.

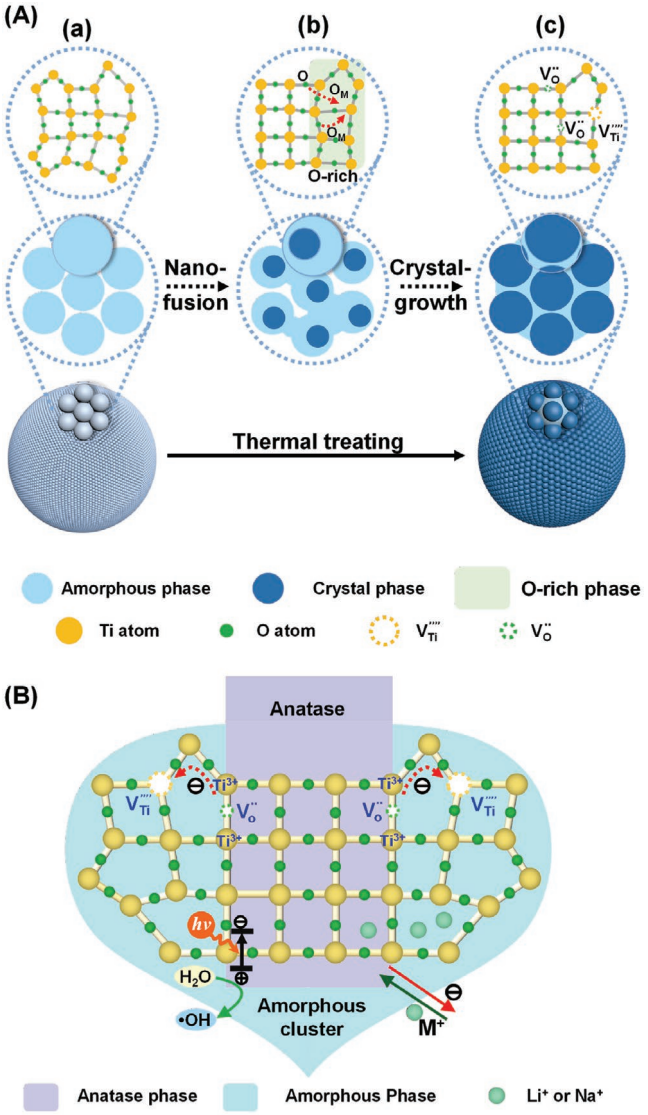

Figure 5. A) The illustration of the formation of the amorphous–anatase TiO_2 from amorphous TiO_2. a–c) refer to the simulated atomic change process from amorphous TiO_2 to amorphous–anatase TiO_2, O_M refers to migrating oxygen. B) Proposed mechanism of the photocatalytic properties and electrochemical properties of the amorphous–crystalline TiO_2.

With the grain-boundary migration from anatase to the amorphous phase, the various O species move to the interface of the amorphous–anatase phase. A relatively low calcination temperature is available to keep the O species in the interface phase (from Figure 5A-a to b, top), which will form an O-rich interface to produce distortions and concomitant Ti vacancies or the so-called p-type state. O species near Ti-vacancies would be O^- to balance the loss of Ti atoms (from Figure 5A-b to c, top). The formation of titanium vacancies can be described as

$$2O_M^x \rightarrow V_{Ti}'''' + 2O_O + 4h^{\bullet} \quad (3)$$

where V''''_{Ti} stands for titanium vacancy, and $h^{\bullet}$ represents hole.

With the calcination time prolonged, the nanocrystals continue to grow, contributing to a larger particle size and nanofusion domains, and form mesopores (from Figure 5A-b to c, middle). Finally, the homojunction of O-vacancies and Ti-vacancies form in the coherent interface of the amorphous–crystalline phase.

With the growth of anatase nanocrystals, the occurrence of Ti-vacancies and O-vacancies at the interface might be a dynamic state/balance. This possible mechanism of an interface homojunction of O-vacancies and Ti-vacancies we propose also accounts for the charge balance because the O-vacancies in the crystalline phase is near Ti-vacancies in the interface phase (see detailed description of the formation of interfacial defects in Supporting Information).

The unique electron-transmission pathway from O-vacancies to Ti-vacancies forms a possible unidirectional conductivity from n-type to p-type, which will not only be beneficial for the separation of electrons and holes in photocatalysis (Figure 5B, left) but also improve the interfacial conduction and favors the transfer of electrons or Li^+/Na^+ (Figure 5B, right). Meanwhile, the amorphous nanoclusters possibly act as a hole trapping center in photocatalysis and provide higher capacity and less structural confinement for Li^+/Na^+ in the insertion/extraction reaction, especially for the large-sized Na^+.

These observations indicate that pure TiO_2 can function in its amorphous-nanocrystal structure without incorporating foreign impurities into/onto the TiO_2 lattice. Experiments and theoretical computations have been conducted to study the homojunction of oxygen and titanium vacancies in TiO_2 and its quite specificities, such as: (i) unique electron pathway from n to p, (ii) atomic-coherent amorphous-nanocrystal homostructures, and (iii) meso-structure for confining-growth. The O-rich interface model formed by migrating oxygen at relatively low temperature is a possible explanation to our homojunction of oxygen and titanium vacancies, although it will still need further characterizations. It is believed that this work provides a new insight for the investigation of the nature of semiconductors and its high-performance design.

Supporting Information

Supporting Information is available from the Wiley Online Library or from the author.

Acknowledgements

This work was supported by National Key R&D Program of China (2017YFC1103800), National SFC (U1662134, U1663225, 51472190, 51611530672, 21711530705, 51503166, 21706199), ISTCP (2015DFE52870), PCSIRT (IRT_15R52), HPNSF (2016CFA033, 2017CFB487), and SKLPPC (PPC2016007).

Conflict of Interest

The authors declare no conflict of interest.

Keywords

energy storage, homojunction of oxygen and titanium vacancy, n–p effect, photocatalysis, titanium dioxide

Received: April 4, 2018
Revised: May 12, 2018
Published online: June 26, 2018

[1] E. J. Crossland, N. Noel, V. Sivaram, T. Leijtens, J. A. Alexander-Webber, H. J. Snaith, *Nature* **2013**, *495*, 215.
[2] J. S. Chen, Y. L. Tan, C. M. Li, Y. L. Cheah, D. Luan, S. Madhavi, F. Y. Boey, L. A. Archer, X. W. Lou, *J. Am. Chem. Soc.* **2010**, *132*, 6124.
[3] X. Li, T. Fan, H. Zhou, S. K. Chow, W. Zhang, D. Zhang, Q. Guo, H. Ogawa, *Adv. Funct. Mater.* **2010**, *19*, 45.
[4] N. Shi, X. Li, T. Fan, H. Zhou, J. Ding, D. Zhang, H. Zhu, *Energy. Environ. Sci.* **2010**, *4*, 172.
[5] S. W. Verbruggen, M. Keulemans, M. Filippousi, D. Flahaut, G. Van Tendeloo, S. Lacombe, J. A. Martens, S. Lenaerts, *Appl. Catal. B: Environ.* **2014**, *156–157*, 116.
[6] P. Kofstad, *Nonstoichiometry, Diffusion, and Electrical Conductivity in Binary Metal Oxides*, Wiley-Interscience, New York **1972**.
[7] H. Matzke, in *Nonstoichiometric Oxides* (Ed: O. T. Sørensen), Academic Press, New York **1981**, p. 155
[8] J. Nowotny, T. Bak, M. Nowotny, L. Sheppard, *J. Phys. Chem. B* **2006**, *110*, 18492.
[9] a) T. Bak, M. K. Nowotny, L. R. Sheppard, J. Nowotny, *J. Phys. Chem. C* **2008**, *112*, 13248; b) M. K. Nowotny, T. Bak, J. Nowotny, *J. Phys. Chem. B* **2006**, *110*, 16270; c) T. Bak, J. Nowotny, M. Rekas, C. C. Sorrell, *J. Phys. Chem. Solids* **2003**, *64*, 1069.
[10] L. Pan, S. Wang, J. Xie, L. Wang, X. Zhang, J. J. Zou, *Nano Energy* **2016**, *28*, 296.
[11] S. Wang, L. Pan, J. J. Song, W. Mi, J. J. Zou, L. Wang, X. Zhang, *J. Am. Chem. Soc.* **2015**, *137*, 2975.
[12] a) T. Xia, W. Zhang, J. B. Murowchick, G. Liu, X. Chen, *Adv. Energy. Mater.* **2013**, *3*, 1516; b) S. Huang, L. Zhang, X. Lu, L. Liu, L. Liu, X. Sun, Y. Yin, S. Oswald, Z. Zou, F. Ding, O. G. Schmidt, *ACS Nano* **2017**, *11*, 821.
[13] X. Li, J. Yu, M. Jaroniec, *Chem. Soc. Rev.* **2016**, *45*, 2603.
[14] J. G. Yu, Y. R. Su, B. Cheng, *Adv. Funct. Mater.* **2010**, *17*, 1984.
[15] E. L. Crepaldi, G. J. de A. A. Soler-Illia, D. Grosso, F. Cagnol, F. Ribot, C. Sanchez, *J. Am. Chem. Soc.* **2003**, *125*, 9770.
[16] X. Y. Yang, L. H. Chen, Y. Li, J. C. Rooke, C. Sanchez, B. L. Su, *Chem. Soc. Rev.* **2017**, *46*, 481.
[17] J. Zhang, Q. Xu, Z. Feng, M. Li, C. Li, *Angew. Chem.* **2008**, *120*, 1790; *Angew. Chem., Int. Ed.* **2008**, *47*, 1766.
[18] J. Yu, J. Low, W. Xiao, P. Zhou, M. Jaroniec, *J. Am. Chem. Soc.* **2014**, *136*, 8839.
[19] I. W. Chen, X. H. Wang, *Nature* **2000**, *404*, 168.
[20] L. S. J. Kang, *Sintering: Densification, Grain Growth, and Microstructure*, Elsevier, Butterworth-Heinemann **2005**.
[21] Y. Lu, X. Cheng, G. Tian, H. Zhao, L. He, J. Hu, S. M. Wu, Y. Dong, G. G. Chang, S. Lenaerts, S. Siffert, G. Van Tendeloo, Z. F. Li, L. L. Xu, X. Y. Yang, B. L. Su, *Nano Energy* **2018**, *47*, 8.
[22] M. Liu, R. Inde, M. Nishikawa, X. Qiu, D. Atarashi, E. Sakai, Y. Nosaka, K. Hashimoto, M. Miyauchi, *ACS Nano* **2014**, *8*, 7229.
[23] N. O. Gopal, H.-H. Lo, S.-C. Sheu, S. C. Ke, *J. Am. Chem. Soc.* **2010**, *132*, 10982.
[24] G. Wu, K. C. Chan, L. Zhu, L. Sun, J. Lu, *Nature* **2017**, *545*, 80.
[25] J. M. Krans, C. J. Muller, N. van der Post, F. R. Postma, A. P. Sutton, T. N. Todorov, J. M. van Ruitenbeek, *Phys. Rev. Lett.* **1995**, *74*, 2146.
[26] X. Y. Yang, G. Tian, L. H. Chen, Y. Li, J. C. Rooke, Y. X. Wei, Z. M. Liu, Z. Deng, G. Van Tendeloo, B. L. Su, *Chem. Eur. J.* **2011**, *17*, 14987.
[27] L. H. Chen, X. Y. Li, G. Tian, Y. Li, H. Y. Tan, G. Van Tendeloo, G. S. Zhu, S. L. Qiu, X. Y. Yang, B. L. Su, *ChemSusChem* **2011**, *4*, 1452.
[28] D. Massiot, F. Fayon, M. Capron, I. King, S. Le Calvé, B. Alonso, J. O. Durand, B. Bujoli, Z. Gan, G. Hoatson, *Magn. Reson. Chem.* **2002**, *40*, 70.
[29] L. Mafra, R. Siegel, C. Fernandez, D. Schneider, F. Aussenac, J. Rocha, *J. Magn. Reson* **2009**, *199*, 111.
[30] J. Ovenstone, K. Yanagisawa, *Chem. Mater.* **1999**, *11*, 2770.
[31] J. Zhang, M. Li, Z. Feng, J. Chen, C. Li, *J. Phys. Chem. B* **2006**, *110*, 927.
[32] S. J. Schiff, K. Jerger, D. H. Duong, T. Chang, M. L. Spano, W. L. Ditto, *Nature* **1994**, *370*, 615.
[33] J. Gleick, *Chaos: Making a New Science*, Open Road Media, **2011**.
[34] X. Yu, B. Kim, Y. K. Kim, *ACS Catal.* **2013**, *3*, 2479.
[35] F. Zuo, L. Wang, T. Wu, Z. Zhang, D. Borchardt, P. Feng, *J. Am. Chem. Soc.* **2010**, *132*, 11856.
[36] V. Mastikhin, I. Mudrakovsky, A. Nosov, *Prog. Nucl. Mag. Res. Sp.* **1991**, *23*, 259.
[37] M. S. Lazarus, T. K. Sham, *Chem. Phys. Lett.* **1982**, *92*, 670.
[38] E. Mccafferty, J. P. Wightman, *Surf. Interface Anal.* **1998**, *26*, 549.
[39] C. N. R. Rao, V. Vijayakrishnan, G. U. Kulkarni, M. K. Rajumon, *Appl. Surf. Sci.* **1995**, *84*, 285.
[40] J. C. Dupin, D. Gonbeau, P. Vinatier, A. Levasseur, *Phys. Chem. Chem. Phys.* **2000**, *2*, 1319.
[41] J. Zou, J. Gao, F. Xie, *J. Alloys Compd.* **2010**, *497*, 420.
[42] J. Moulder, in *Handbook of X-Ray Photoelectron Spectroscopy: A Reference Book of Standard Spectra for Identification and Interpretation of XPS Data* (Eds: J. Chastain, R. C. King), Physical Electronics Division, Perkin-Elmer Corporation, Eden Prairie, MN **1992**.
[43] a) V. Berube, G. Radtke, M. Dresselhaus, G. Chen, *Int. J. Energy Res.* **2007**, *31*, 637; b) A. P. Alivisatos, *J. Phys. Chem.* **1996**, *100*, 13226.
[44] F. A. Kröger, H. J. Vink, in *Solid State Physics* (Eds: F. Seitz, D. Turnbull), Academic Press, New York, **1956**.

